Structure, morphology and magnetic properties of flowerlike gamma-Fe2O3@NiO core/shell nanocomposites synthesized from different precursor concentrations

He, Xuemin; Zhang, Chuangwei; Guo, Fangfang; Zhou, Qinghai; Li, Yongtao; Zhang, Hongguang; Liu, Liqing; Du, Youwei; Zhong, Wei

Published in:
Materials Research Bulletin

DOI:
10.1016/j.materresbull.2019.110495

Publication date:
2019

Materials Research Bulletin 118 (2019) 110495

Contents lists available at ScienceDirect

Materials Research Bulletin

journal homepage: www.elsevier.com/locate/matresbu

Structure, morphology and magnetic properties of flowerlike γ-Fe_2O_3@NiO core/shell nanocomposites synthesized from different precursor concentrations

Xuemin He[a,b], Chuangwei Zhang[a], Fangfang Guo[c], Qinghai Zhou[d], Yongtao Li[a,*], Hongguang Zhang[a], Liqing Liu[a], Youwei Du[b], Wei Zhong[b,*]

[a] New Energy Technology Engineering Laboratory of Jiangsu Province, Research Center of Information Physics and School of Science, Nanjing University of Posts and Telecommunications, Nanjing, 210023, PR China
[b] National Laboratory of Solid State Microstructures, Nanjing University, Nanjing, 210093, PR China
[c] Zernike Institute for Advanced Materials, Faculty of Science and Engineering, University of Groningen, Groningen, 9747 AG, the Netherlands
[d] School of Computing Informatics & Decision Systems Engineering, Arizona State University, Tempe, AZ, 85281, USA

ARTICLE INFO

Keywords:
Precursor concentration
Microstructure
Interface
Freezing temperature
Exchange bias

ABSTRACT

The flowerlike γ-Fe_2O_3@NiO core/shell nanocomposites are synthesized by the two-step method. Their structure and morphology can be controlled by tuning the precursor concentration. Microstructural analysis reveals that all the samples have distinct core/shell structure without impurities, and the NiO shells are built of many irregular nanosheets which enclose the surface of γ-Fe_2O_3 core. As the precursor concentration decreases (i.e., more NiO content), the NiO grain grows significantly, and the thickness of NiO shells increases. Magnetic experiments are performed to analyze the influences of different microstructures on magnetic properties of samples and we have the following two results. First, at 5 K, along with increasing thickness of NiO shell, the saturation magnetization increases, while the residual magnetization decreases slightly. Second, the hysteresis loops under cooling field demonstrate that the value of exchange bias effect fluctuates between 13 Oe and 17 Oe. This is mainly because of the NiO shell that (i) is composed of irregular nanosheets with disordered orientations, and (ii) does not form a complete coating around γ-Fe_2O_3 core.

1. Introduction

Magnetic nanoparticles (NPs) have been widely investigated because of advantages in both fundamental research and application potentials in a variety of high-impact fields including information technology, catalysis, magnetic sensing and nanoscale electronic [1–6]. Especially, for the magnetic nanocomposites with typical core/shell structure and good interfacial anisotropy, they have key property of the exchange coupling system, which results in the exchange bias (EB) effect and enhanced coercivity (H_C) [7,8]. Since the discovery of EB effect in Co@CoO NPs by Meiklejohn and Bean in 1956 [9,10], EB-based core/shell nanocomposites with various microstructures have been extensively reported.

The conventional exchange coupling between antiferromagnet (AFM) and ferromagnet (FM) or ferrimagnet (FiM) occurs at the F(i)M-AFM interface, where the hysteresis loop shifts (i.e., H_E) along the field axis after field cools down from above the Néel temperature (i.e., T_N) of AFM. For instance, the EB coupling exhibited by $Fe_{3-\delta}O_4$@CoO core/shell nanocomposites is closely correlated to their assembly structure, accompanied by the strong influence of interparticle interaction on their intrinsic magnetic properties [11]. The study on 50 nm $CoCr_2O_4$ particles with core/shell structure reveals that memory effect and EB effect are temperature-dependent [12]. In addition, Gandha et al. point out that the giant EB in Co/CoO core-shell nanowire assemblies has an angular dependence on the value of EB field and the direction of magnetization [13]. Recently, it has been reported that highly homogeneous and inverted core/shell magnetic nanocomposites which demonstrate significant EB effect can be synthesized by simple chemical methods, such as FeO/Fe_3O_4 [14–16], CoO/γ-Fe_2O_3 [17,18], MnO/γ-Mn_2O_3 [19,20], and MnO/Mn_3O_4 systems [20,21].

All the researches above indicate that the exchange coupling of core/shell nanocomposites are highly dependent on shape, size, composition, surface volume ratio, and interfacial characteristics. In order to control these factors, an effective method is to change the precursor

* Corresponding authors.
E-mail addresses: liyt@njupt.edu.cn (Y. Li), wzhong@nju.edu.cn (W. Zhong).

https://doi.org/10.1016/j.materresbull.2019.110495
Received 9 February 2019; Received in revised form 15 May 2019; Accepted 20 May 2019
Available online 21 May 2019

concentration. For example, Khurshid et al. have reported that the shape of core/shell FeO/Fe_3O_4 nanocomposites could be controlled by altering the molar ratios of different capping agents [14], and the particles will exist cubical, spherical, octopod, clavillose or triangular morphology in shapes. Pajor-Swierzy et al. discuss the influence of the concentration of Ag precursor on the properties of nickel-silver core/shell nanocomposites [22]. Based on the wet chemistry synthetic method, Sanles-Sobrido et al. have found that the magnetic properties of spherical core-shell nanostructures are tunable, which can be achieved by tailoring the weight ratio of Ni:PS (where PS refers to the polystyrene) [23]. In our previous work, we have successfully controlled the Ni content in the Ni-NiO nanocomposites by tuning precursor concentration [24]. Therefore, the EB effect and the corresponding phenomenon can be accurately regulated by the microstructures of the nanocomposites.

In this paper, we select the γ-Fe_2O_3/NiO system as a research object from numerous combinations because NiO has high T_N and satisfactory stability, and γ-Fe_2O_3 has excellent magnetic properties. We report the two-part seed-mediated synthesis of flowerlike γ-Fe_2O_3@NiO core/shell nanocomposites. During the process of sample preparation, nanocomposites consist of a fixed FiM γ-Fe_2O_3 core surrounded by AFM NiO shells in different thicknesses. The roles of the precursor concentration which is critical to the structure and morphology are examined systemically, and the magnetic properties of the flowerlike γ-Fe_2O_3@NiO core/shell nanocomposites are further investigated in detail.

2. Experimental details

2.1. Sample preparation

Throughout the sample preparation procedure, iron oxide (Fe_3O_4) spheres are synthesized first. Typically, 0.811 g (5 mmol) of Iron(III) chloride is dissolved in 40 mL of ethylene glycol (EG), then 3.6 g of sodium acetate and 1.0 g of polyethylene glycol (PEG 4000) are successively added to the solution, followed by a step of stirring the solution for 20 min. The obtained clear solution is transferred to an autoclave, and is placed in a moistureless box. Then the reaction happens at 200 °C with a heating rate of 5 °C/min for a duration of 8 h, and then the resultants are cooled down to room temperature. The black precipitate is washed by ethanol and distilled water, and kept in a moistureless box at 80 °C for 12 h. Finally, the black powder products formed by grinding the precipitate are Fe_3O_4 microspheres.

In the second step, 0.291 g (1 mmol) of Nickel(II) nitrate hexahydrate is added to a mixed solution of 7 mL of alcohol and 3 mL of EG, which forms a solution in a light green color. Then 0.232 g (1 mmol) of Fe_3O_4 powder is added to the solution which is then ultrasonically dispersed for approximately 15 min. The obtained mixture is transferred to an autoclave and kept in a moistureless box, and reacts at 160 °C with a heating rate of 5 °C/min for 8 h followed by a procedure of naturally cooling down to room temperature. The black precipitate is washed several times by ethanol and distilled water, and is kept in a moistureless box at 80 °C for 12 h to produce $Fe_3O_4/Ni(OH)_2$ core/shell nanocomposites. Then, the product is calcined in air at 300 °C with a heating rate of 5 °C/min for 3 h in a tube furnace.

Herein, the ultimately obtained γ-Fe_2O_3@NiO sample is marked as 1/1. Noting that the morphology of flowerlike γ-Fe_2O_3@NiO core/shell nanocomposites can be governed by tuning the precursor concentration (i.e., the molar ratio of Fe_3O_4 to Nickel(II) nitrate hexahydrate). Therefore, the other samples could be produced by simply altering the concentration to 1/0.2, 1/0.5, 1/2, 1/3, 1/5 and 1/7, respectively. Moreover, the sample denoted as 1/7–400 °C is obtained by a similar synthesis process, where the precursor concentration is 1/7 and the temperature of calcining is extended to 400 °C.

2.2. Characterization

The crystal structures of products are characterized by X-ray diffraction (XRD) using a Bruker D8 Advance A25 with Cu Kα radiation (λ = 1.54056 Å) in the range of 20°-70°. X-ray photoelectron (XPS) spectra are collected using PREVAC XR408 spectrometer. Particle shapes are imaged with HITACHI S4800 scanning electron microscope (SEM). For transmission electron microscope (TEM) investigation, a drop of tested powder sample in ethanol is deposited on each carbon-coated copper grid and then dried in the air. Based on the Hitachi HT7700 instrument, high-resolution TEM (HRTEM) analyses are used to determine local microstructure. Raman spectra are recorded in the range of 400-1150 cm^{-1} by using a confocal spectrograph (Invia, Renishaw, England) with an excitation wavelength of 632.8 nm. Magnetic measurements are conducted using a superconducting quantum interference device (SQUID) magnetometer (Quantum Design, MPMS-XL5), which mainly includes the following two aspects: (i) low-temperature (5 K) hysteresis (*M-H*) loops under zero-field-cooling (ZFC) and field-cooling (FC, from 300 K in a field of H_{cool} = 50 kOe); and (ii) ZFC and 100 Oe FC magnetization (*M-T*) curves in the temperature ranging from 5 K to 300 K.

3. Results and discussion

3.1. Structure and morphology

Fig. 1 presents the XRD patterns of the γ-Fe_2O_3@NiO nanocomposites obtained under different precursor concentrations. The typical

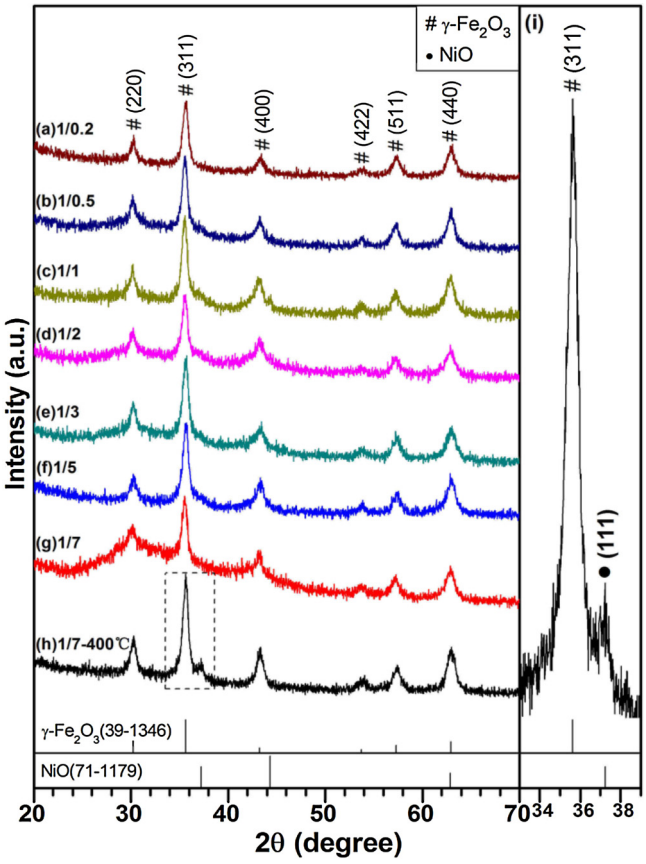

Fig. 1. XRD patterns of γ-Fe_2O_3@NiO core/shell nanocomposites formed in different precursor concentrations: (a) 1/0.2; (b) 1/0.5; (c) 1/1; (d) 1/2; (e) 1/3; (f) 1/5; (g) 1/7; and (h) shows the XRD pattern of an extra sample (1/7) with higher calcination temperature of 400 °C. The right region (i) shows the enlarged view of (h) in the 33-39° 2θ range.

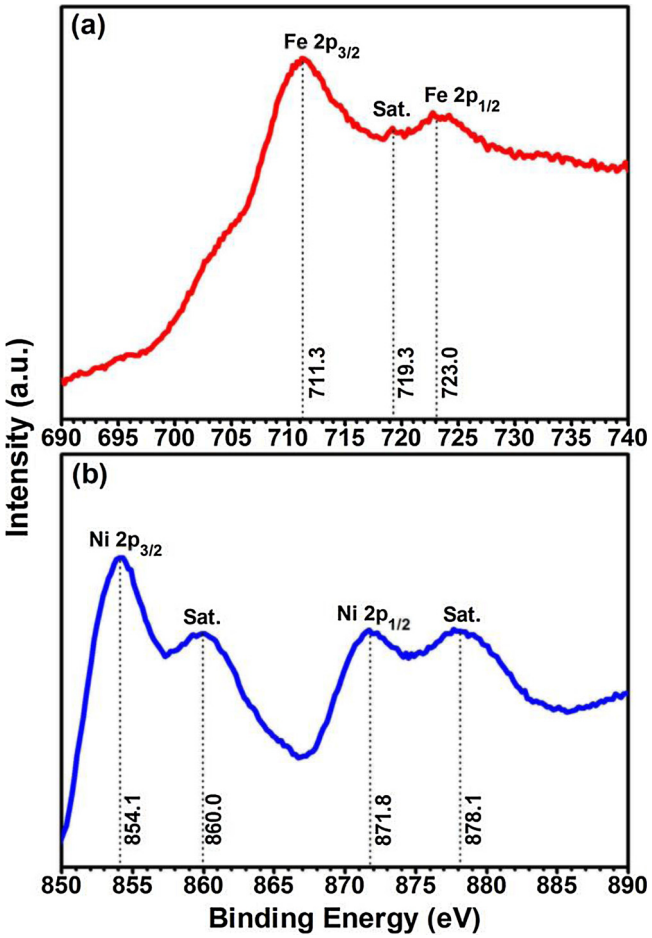

Fig. 2. XPS spectra of (a) Fe 2p and (b) Ni 2p region for the γ-Fe_2O_3@NiO core/shell nanocomposites formed in precursor concentration of 1/5.

(220), (311), (400), (511) and (440) diffraction peaks are perfectly matched with γ-Fe_2O_3 phase (JCPDS no. 39-1346), while peaks of NiO phase are not apparently observed. However, as the calcination temperature of Fe_3O_4@$Ni(OH)_2$ nanocomposites increases to 400 °C, NiO peaks can be observed in the 1/7–400 °C sample, as shown in Fig. 1(h). It is interpreted that the increase of calcination temperature contributes to the improvement of crystallinity and the growth of grains. Fig. 1(i) is the enlarged view of Fig. 1(h) in the range of 33°-39°, it presents the typical (111) diffraction peak of NiO phase (JCPDS no. 71-1179). According to the analysis of XRD patterns, no other crystalline impurities are detected. Unfortunately, the XRD patterns neither indicate obvious differences among several samples nor recognized the NiO component distinctly.

Considering that it is difficult to distinguish maghemite (γ-Fe_2O_3) from magnetite (Fe_3O_4) through XRD pattern [25,26], XPS analysis of the 1/5 sample is then performed to better assess the chemical nature of the nanocomposites. Fig. 2(a) shows the XPS spectrum of Fe 2p region, in which the two peaks at 711.3 eV and 723.0 eV are correspond to the Fe 2p 3/2 and Fe 2p 1/2 binding energies, respectively. Furthermore, the satellite peak that appears near 719.3 eV is the characteristic peak of γ-Fe_2O_3 [27–29], which is different from Fe_3O_4. As shown in Fig. 2(b), the XPS spectrum of Ni 2p region includes two broad sets of signals, and corresponds to 2p 3/2 (854.1 eV with its satellite peak at 860.0 eV) and 2p 1/2 (871.8 eV with its satellite peak at 878.1 eV) [23,30], respectively. The nickel oxidation states are highly correlated to the energy gaps between the Ni 2p main peak and its satellite peak. These information demonstrates that there is no agreement with the spectra of Ni_2O_3, and nickel is involved in both samples in the form of Ni^{2+}, consequently excluding the presence of metallic nickel (778.0 eV).

Eight representative SEM images of flowerlike γ-Fe_2O_3@NiO nanocomposites are presented in Fig. 3, which demonstrates the typical core/shell structures. It is remarkable that the thickness of the NiO shell changes along with the change of the concentration of the nickel source. Among them, the NiO shell is made of irregular nanosheets. Although it seems that the sheet-like NiO encloses the γ-Fe_2O_3 core, NiO is actually inserted at the surface of core, which forms a flower shape. It has already been noted above that NiO is not detected in the above XRD patterns. Furthermore, with the increase of Ni^{2+} ion concentration, the flowerlike NiO shell becomes thicker and more conspicuous, and finally the surface tends to be stable due to the limited adsorption capacity of Fe_3O_4. For an overview of sample sizes, we have performed statistical measurements for the diameter of each nanoparticle using the Nano Measurer software, and the average diameter of the samples formed in different precursor concentrations varies from 328 ± 15 nm to 386 ± 19 nm. To summarize, the above analysis indicates that the precursor concentration has a significant influence on the morphology of γ-Fe_2O_3@NiO core/shell nanocomposites.

Based on the above analysis of XRD, XPS and SEM data, it is confirmed that the products obtained from current reactions are flowerlike γ-Fe_2O_3@NiO core/shell nanocomposites. From the SEM images, we can conclude that the morphology of the samples formed in different precursor concentrations changes slightly. The analysis below will address the four samples obtained in the concentrations of 1/1, 1/2, 1/5 and 1/7, respectively.

To explore the microstructure of samples, especially for the core/shell structure, the TEM images of the four samples form concentrations of 1/1, 1/2, 1/5 and 1/7 are measured, as shown in Fig. 4(a)–(d). Obviously, all the samples are core/shell structured: the big black balls are the cores, γ-Fe_2O_3 microspheres, and the peripheral gray sheets are the shells, NiO nanosheets, forming a flowerlike γ-Fe_2O_3@NiO core/shell composite. Similar morphology is also observed by Sanles-Sobrido et al. in the spherical PS/Ni microspheres/nanoshells composites [23]. To get a better view about the sizes of core and shell, the TEM images of few particles (for example, two) for the same four γ-Fe_2O_3@NiO

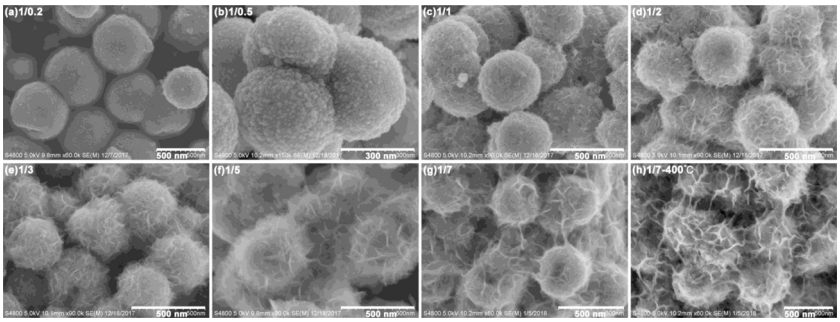

Fig. 3. SEM images of γ-Fe_2O_3@NiO core/shell nanocomposites formed in different precursor concentrations: (a) 1/0.2; (b) 1/0.5; (c) 1/1; (d) 1/2; (e) 1/3; (f) 1/5; (g) 1/7; and (h) shows the SEM image of an extra sample (1/7) with higher calcination temperature of 400 °C.

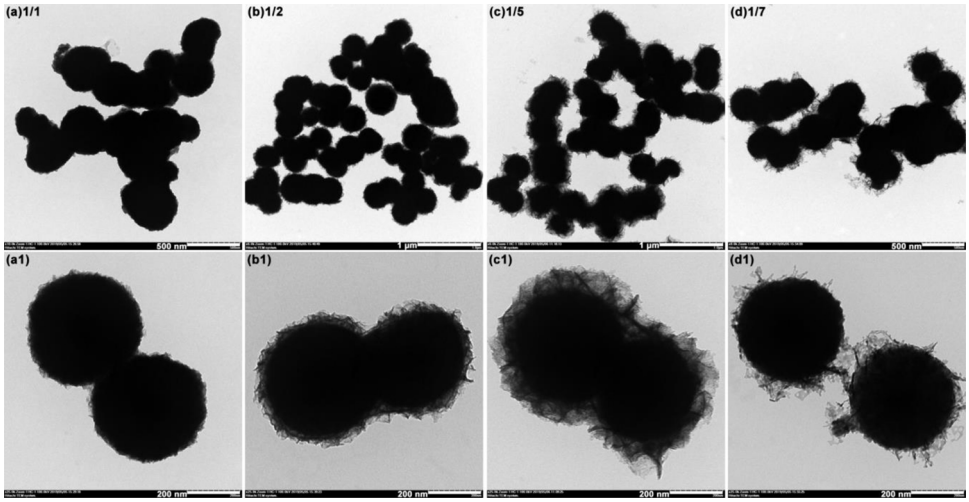

Fig. 4. TEM images of γ-Fe_2O_3@NiO core/shell nanocomposites formed in different precursor concentrations: (a) 1/1, (b) 1/2, (c) 1/5, (d) 1/7; (a1)-(d1) show the corresponding TEM images of two particles at high magnification.

samples are recorded at high magnification (for example, ×25 k), as shown in Fig. 4(a1)–(d1). First, for γ-Fe_2O_3 core, the shape and size of microspheres can be basically considered to maintain invariable with the change of precursor concentration. The reason is because γ-Fe_2O_3 cores all come from the evolution of the same seeds (Fe_3O_4 microspheres), and the calcination conditions of the intermedium (Fe_3O_4@Ni$(OH)_2$ core/shell composites) are identical (namely, 5 °C/min, 300 °C, 3 h). Secondly, for NiO shells which are consisted of multiple irregular nanosheets with disordered orientations, as precursor concentration changes from 1/1 to 1/5, the average thickness of NiO shells increase markedly with an enhancement of the compactness of NiO shells. However for the γ-Fe_2O_3@NiO sample formed in 1/7 concentration, NiO shells begin to peel, thin, and form some scattered nanosheets instead of complete coatings around γ-Fe_2O_3 core. This is mainly because the surface tends to stabilize due to the limited adsorption capacity of Fe_3O_4 microspheres with the increase of Ni^{2+} ion concentration in reaction. The excessive Ni^{2+} ions enlarge NiO nanosheets which become heavier and heavier so that the obtained NiO shell enclosing the surface of γ-Fe_2O_3 core start to break down and finally result in the incomplete core/shell structure. Above TEM results are consistent with those of SEM and further demonstrated the core/shell structure of γ-Fe_2O_3@NiO samples.

In order to further evaluate the impact of precursor concentration on the structure, the results of Raman spectra of the γ-Fe_2O_3@NiO nanocomposites are presented in Fig. 5. The features at 491.3 cm^{-1} and 690.2 cm^{-1} are due to γ-Fe_2O_3 [31], while all the other Raman features represent the characteristics of NiO [32]. The peaks of iron oxide further demonstrate that the core is completely composed of γ-Fe_2O_3 instead of Fe_3O_4. Obviously, both of the two peaks for all four samples are consistent, which corresponds to the fact that precursor concentration has not affected Raman mode of γ-Fe_2O_3 core much, consistent with the previous XRD, SEM and TEM analysis. As the precursor concentration decreases, the peak at 1177.6 cm^{-1} of NiO becomes higher, indicating that the amount of NiO on the surface of the nanocomposites increases, which also proves the SEM/TEM analysis.

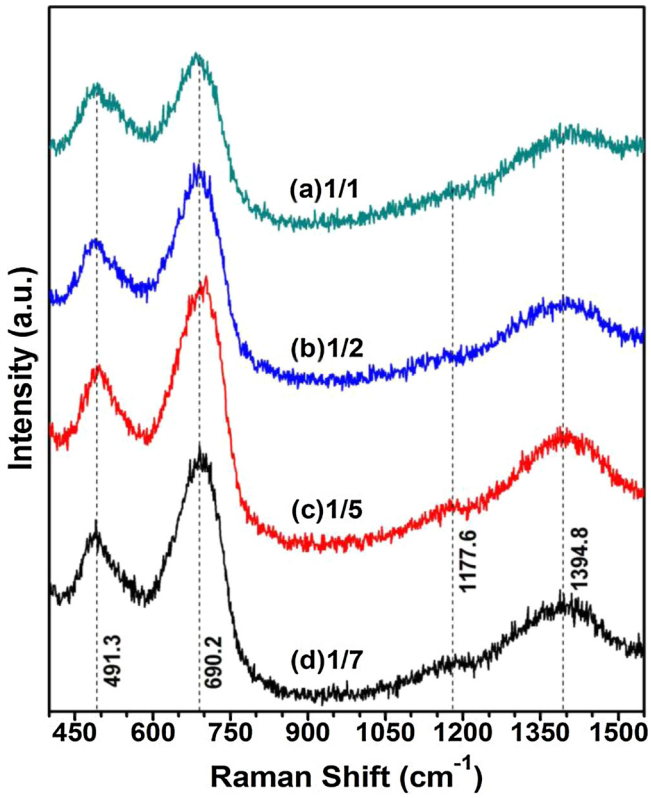

Fig. 5. Raman spectra of γ-Fe_2O_3@NiO core/shell nanocomposites formed in different precursor concentrations: (a) 1/1; (b) 1/2; (c) 1/5; (d) 1/7.

3.2. Magnetic properties

The effect of nanocomposites morphology on the magnetic properties is evaluated by SQUID. In a magnetic field of 100 Oe, the temperature-dependent magnetization (*M-T*) curves are measured under ZFC and FC from 300 K to 5 K. M_{ZFC} is measured when the sample of nanocomposites are heated from 5 K to 300 K, whereas M_{FC} is recorded during the subsequent cooling procedure. Fig. 6 presents the main results for the γ-Fe_2O_3@NiO granular system. An irreversible magnetic behavior (splitting between the FC and ZFC curves) is observed in the whole temperature range and the irreversibility occurs when $T > 300$ K in all curves. This behavior indicates that a strong FiM/AFM exchange coupling exists in this granular system. As temperature increases, M_{ZFC} also increases while M_{FC} decreases on the contrary. The bifurcation between ZFC and FC curves is explained by the possible freezing of disordered uncompensated surface spins. It is well known that the value of T_B depends on the applied magnetic field [33]. In this situation, the maximum is not observed in the ZFC curve, which means that T_B is above 300 K under an applied field of 100 Oe. Similar results are also observed in Fe/Fe-Oxide [34], Co-B NPs [35], Ni/NiO nanostructures

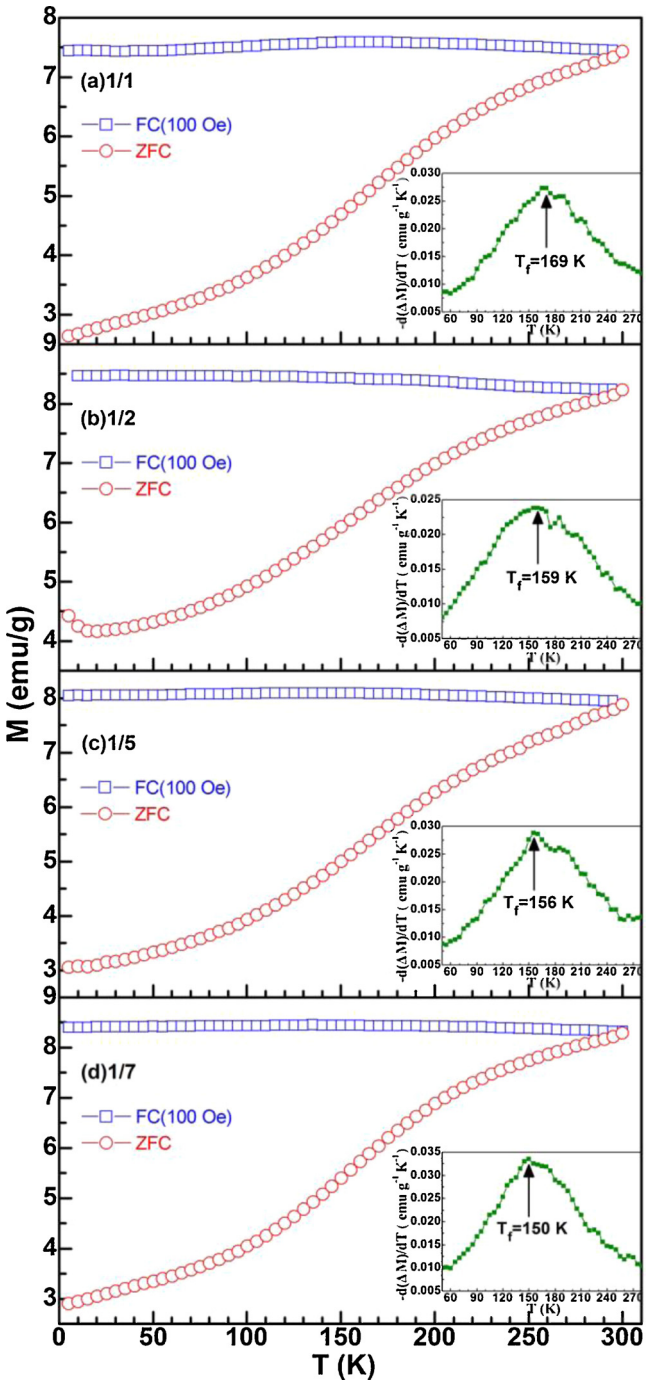

Fig. 6. ZFC and 100 Oe FC magnetization (*M-T*) curves of γ-Fe_2O_3@NiO core/shell nanocomposites formed in different precursor concentrations: (a) 1/1; (b) 1/2; (c) 1/5; (d) 1/7. Insets show the temperature derivative of the difference between the FC and ZFC magnetizations.

[33,36] and PS/Ni nanocomposites [23]. The partial magnetic behavior of the NiO-containing system can usually be explained by the disordered NiO component. The insets in Fig. 6 present the derivative of the difference between the FC and ZFC magnetizations with respect to temperature, i.e., -d(M_{FC}-M_{ZFC})/dT, which provides qualitative evaluation on the magnetic behaviors of nanosystem [34]. The peak located at T_f suggests that there is a frozen disordered magnetic state when the temperature is below the following, T_f = 169, 159, 156, and 150 K, respectively. As precursor concentration decreases, i.e., as the volume of NiO content increases, the value of T_f decreases monotonously from 169 K to 150 K, which demonstrates that at low temperature, the ferromagnetic moment is in a blocked state and a frozen magnetic state is formed in the FiM/AFM nanocomposites system.

As shown in Fig. 7, hysteresis loops under ZFC and FC are measured at 5 K. In the ZFC and FC measurements, the sample is cooled down in a zero field and an applied field of 50 kOe, respectively, and then the magnetization is measured. We can observe that the shape of the ZFC and FC loops are similarly given a relatively small coercivity listed in Table 1. Both ZFC and FC loops indicate that the value of saturation magnetization monotonously increases (M_s = 55.4, 57.8, 59.3 and 60.1 emu/g, respectively) in four samples as a consequence of larger volume of NiO in the latter samples. From the insets which present the enlarged view near the origin of hysteresis loops, we have the following observations. First, the hysteresis loops under ZFC illustrate a typical hysteresis loop which is perfectly symmetrical about the two axes. Second, compared with the hysteresis loop under ZFC, the loop under FC shows a significant horizontal offset for each sample, which is characteristic of EB effect accompanied by an enhancement of coercivity [37]. The main reason of such a phenomenon is that the AFM (NiO) spin pins the FiM (γ-Fe_2O_3) spin at the FiM/AFM interface, which is motivated by the magnetic field applied during the cooling procedure. The NiO shell acts as a pinning layer, leading to a unidirectional anisotropy or a preferred direction of magnetization in γ-Fe_2O_3 core. The result of this unidirectional anisotropy is that it is much more difficult to switch the magnetization of the γ-Fe_2O_3 in the opposite direction of the cooling field than to switch it back to the direction of cooling field. It can be quantified as exchange bias field which is calculated by the following formula, $H_E = (H_{C1}-H_{C2})/2$, where H_{C1} and H_{C2} denote the negative and positive coercive fields, respectively. In all samples, the value of H_E is between 13 Oe and 17 Oe, because the flowerlike NiO shell is sheet-like and does not form a complete coating, and the fluctuating value of H_E depends on the microstructural characteristics such as size, phase content and interface roughness. The enhancement of coercivity is defined by the difference of coercivity under FC and ZFC processes, i.e., $\Delta H_C = H_C$(FC) - H_C(ZFC) (ΔH_C = 30, 26, 25 and 41 Oe, respectively) [38]. The specific phenomenon also originates from coupling effect which allows a variety of reversal paths for the spins upon cycling the applied field [33].

4. Conclusions

Flowerlike γ-Fe_2O_3@NiO core/shell nanocomposites with distinct microstructures can be successfully prepared by altering the precursor concentration, and the corresponding structure, morphology and magnetic properties have been systematically investigated through XRD, XPS, SEM, TEM, Raman, and SQUID tools. All the samples exhibit typical core/shell structures, and the precursor concentration has a significant influence on the microstructure, e.g., as the precursor concentration decreases, the NiO shell layer becomes thicker and denser. At 5 K, the saturation magnetization increases along with the increase of the thickness of the NiO shell layer, while the residual magnetization shows a minor decrease as the thickness increases, which is consistent with the antiferromagnetic characteristics of NiO. At the same time, there is a significant exchange coupling in flowerlike γ-Fe_2O_3@NiO core/shell nanocomposites, resulting in the exchange bias effect and enhancement of the coercivity. The value of exchange bias field ranges from 13 Oe to 17 Oe in four samples, because the NiO shell is composed of irregular nanosheets, which are inserted into the surface of γ-Fe_2O_3 core, and therefore does not form a complete coating. It also proves that the structure of FiM-AFM interface has significant impacts on the magnetic properties of γ-Fe_2O_3@NiO core/shell nanocomposites.

Acknowledgements

We would like to thank Engineer Liya Lü of Nanomagnetism Research Group, Nanjing University for SQUID measurement. This

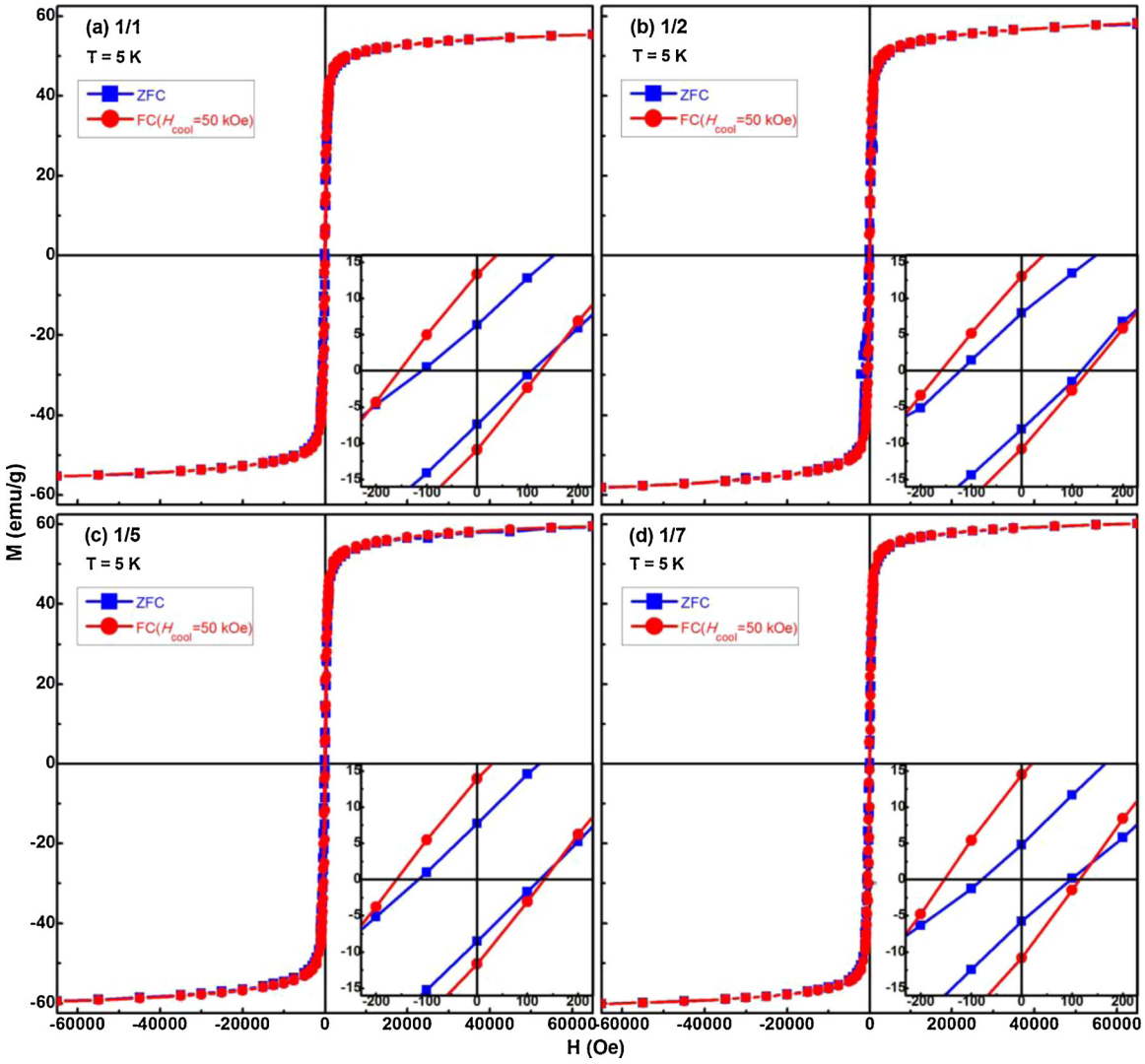

Fig. 7. 5 K hysteresis (*M-H*) loops of γ-Fe_2O_3@NiO core/shell nanocomposites formed in different precursor concentrations: (a) 1/1; (b) 1/2; (c) 1/5; (d) 1/7. Inset: an enlargement of the loops around origin.

Table 1
Results of the analysis of the magnetic properties for γ-Fe_2O_3@NiO core/shell nanocomposites formed in different precursor concentrations *C*: (a) 1/1; (b) 1/2; (c) 1/5; (d) 1/7.

C	T_f (K)	T = 5 K				
		M_s (emu/g)	H_C(ZFC) (Oe)	H_C(FC) (Oe)	H_E (Oe)	ΔH_C (Oe)
1/1	169	55.4	112	142	13	30
1/2	159	57.8	120	146	14	26
1/5	156	59.3	122	147	17	25
1/7	150	60.1	95	136	14	41

work was financially supported by the National Natural Science Foundation (Grant Nos. 11604160, 11474151 and 11605092), the Natural Science Foundation of Jiangsu Province (Grant No. BK20160876), the Scientific Research Foundation of Nanjing University of Posts and Telecommunications (NUPTSF, Grant Nos. NY215063 and NY217096), and the Open Project for National Laboratory of Solid State Microstructures, Nanjing University (Grant No. M30007), P. R. China.

Appendix A. Supplementary data

Supplementary material related to this article can be found, in the online version, at doi:https://doi.org/10.1016/j.materresbull.2019.110495.

References

[1] Q. Zhao, Z.H. Yan, C.C. Chen, J. Chen, Chem. Rev. 117 (2017) 10121–10211.
[2] R. Hao, R.J. Xing, Z.C. Xu, Y.L. Hou, S. Gao, S.H. Sun, Adv. Mater. 22 (2010) 2729–2742.
[3] S. Singamaneni, V.N. Bliznyuk, C. Binek, E.Y. Tsymbal, J. Mater. Chem. 21 (2011) 16819–16845.
[4] A. Aijaz, J. Masa, C. Rösler, W. Xia, P. Weide, A.J.R. Botz, R.A. Fischer, W. Schuhmann, M. Muhler, Angew. Chem. Int. Ed. 55 (2016) 4087–4091.
[5] I. Almeida, S.G. Mendo, M.D. Carvalho, J.P. Correia, A.S. Viana, Electrochim. Acta 188 (2016) 1–12.
[6] H.M.A. Amin, H. Baltruschat, D. Wittmaier, K.A. Friedrich, Electrochim. Acta 151 (2015) 332–339.
[7] J. Sort, J. Nogués, S. Suriñach, J.S. Muñoz, M.D. Baró, E. Chappel, F. Dupont, G. Chouteau, Appl. Phys. Lett. 79 (2001) 1142–1144.
[8] J. Sort, S. Suriñach, J.S. Muñoz, M.D. Baró, J. Nogués, G. Chouteau, V. Skumryev, G.C. Hadjipanayis, Phys. Rev. B 65 (2002) 174420.
[9] W.H. Meiklejohn, C.P. Bean, Phys. Rev. 102 (1956) 1413–1414.
[10] W.H. Meiklejohn, C.P. Bean, Phys. Rev. 105 (1957) 904–913.
[11] M. Dolci, Y. Liu, X.J. Liu, C. Leuvrey, A. Derory, D. Begin, S. Begin-Colin, B.P. Pichon, Adv. Funct. Mater. 28 (2018) 1706957.
[12] G.J. Kumar, C. Rath, Magn. Magn. Mater. 466 (2018) 69–74.
[13] K. Gandha, R.P. Chaudhary, J. Mohapatra, A.R. Koymen, J.P. Liu, Phys. Lett. A 381 (2017) 25–26.
[14] H. Khurshid, W.F. Li, S. Chandra, M.H. Phan, G.C. Hadjipanayis, P. Mukherjee, H. Srikanth, Nanoscale 5 (2013) 7942–7952.

[15] P. Tancredi, P.C.R. Rojas, O. Moscoso-Londono, U. Wolff, V. Neu, C. Damm, B. Rellinghaus, M. Knobel, L.M. Socolovsky, New J. Chem. 41 (2017) 15033–15041.
[16] X.L. Sun, N.F. Huls, A. Sigdel, S.H. Sun, Nano Lett. 12 (2012) 246–251.
[17] I. Panagiotopoulos, G. Basina, V. Alexandrakis, E. Devlin, G. Hadjipanayis, L. Colak, D. Niarchos, V. Tzitzios, J. Phys. Chem. C 113 (2009) 14609–14614.
[18] C. Liu, J.G. Cui, X.M. He, H.G. Shi, J. Nanopart. Res. 16 (2014) 2320.
[19] I.V. Golosovsky, G. Salazar-Alvarez, A. López-Ortega, M.A. González, J. Sort, M. Estrader, S. Suriñach, M.D. Baró, J. Nogués, Phys. Rev. Lett. 102 (2009) 247201.
[20] A. López-Ortega, D. Tobia, E. Winkler, I.V. Golosovsky, G. Salazar-Alvarez, S. Estradé, M. Estrader, J. Sort, M.A. González, S. Suriñach, J. Arbiol, F. Peiró, R.D. Zysler, M.D. Baró, J. Nogués, J. Am. Chem. Soc. 132 (2010) 9398–9407.
[21] N.N. Song, H.T. Yang, Y. Luo, X. Ren, J. Zhou, S. Geng, G.P. Zhao, X.Q. Zhang, Z.H. Cheng, AIP Adv. 7 (2017) 045316.
[22] A. Pajor-Swierzy, D. Gawel, E. Drzymala, R. Socha, M. Parlinska-Wojtan, K. Szczepanowicz, P. Warszynski, Nanotechnology 30 (2019) 015601.
[23] M. Sanles-Sobrido, M. Bañobre-López, V. Salgueiriño, M.A. Correa-Duarte, B. Rodríguez-González, J. Rivas, L.M. Liz-Marzán, J. Mater. Chem. 20 (2010) 7360–7365.
[24] X.J. Yao, X.M. He, X.Y. Song, Q. Ding, Z.W. Li, W. Zhong, C.-T. Au, Y.W. Du, Phys. Chem. Chem. Phys. 16 (2014) 6925–6930.
[25] Q.K. Ong, X.M. Lin, A. Wei, J. Phys. Chem. C: Nanomater. Interface 115 (2011) 2665–2672.
[26] R.M. Cornell, U. Schwertmann, The Iron Oxides: Structure, Properties, Reactions, Occurrence and Uses, Wiley-VCH, Weinheim, 1996.
[27] X.W. Teng, D. Black, N.J. Watkins, Y. Gao, H. Yang, P Nano Lett. 3 (2003) 261–264.
[28] T. Yamashita, P. Hayes, Appl. Surf. Sci. 254 (2008) 2441–2449.
[29] G.B. Sun, B.X. Dong, M.H. Cao, B. Wei, C. Hu, Chem. Mater. 23 (2011) 1587–1593.
[30] A.N. Mansour, Surf. Sci. Spectra 3 (1998) 231.
[31] G.V.M. Jacintho, P. Corio, J.C. Rubim, J. Electroanal. Chem. 603 (2007) 27–34.
[32] N. Mironova-Ulmane, A. Kuzmin, I. Sildos, M. Pärs, Cent. Eur. J. Phys. 9 (2011) 1096–1099.
[33] H. Ahmadvand, H. Salamati, P. Kameli, F.S. Razavi, J. Supercond. Nov. Magn. 23 (2010) 1467–1471.
[34] L. Del Bianco, D. Fiorani, A.M. Testa, E. Bonetti, L. Savini, S. Signoretti, Phys. Rev. B 66 (2002) 174418.
[35] A.B. Dávila-Ibáñez, J.L. Legido-Soto, J. Rivas, V. Salgueiriño, Phys. Chem. Chem. Phys. 13 (2011) 20146–20154.
[36] L. Del Bianco, F. Boscherini, A.L. Fiorini, M. Tamisari, F. Spizzo, M.V. Antisari, E. Piscopiello, Phys. Rev. B 77 (2008) 094408.
[37] R.H. Kodama, S.A. Makhlouf, A.E. Berkowitz, Phys. Rev. Lett. 79 (1997) 1393–1396.
[38] J. Nogués, J. Sort, V. Langlais, V. Skumryev, S. Suriñach, J.S. Muñoz, M.D. Baró, Phys. Rep. 422 (2005) 65–117.